IEEE Photonics Journal
An IEEE Photonics Society Publication

Open Access

Titanium Dioxide Langmuir–Blodgett Film Saturable Absorber for Passively Q-switched Nd:$GdVO_4$ Laser

Volume 11, Number 2, April 2019

Xi Wang
Yonggang Wang
Yuzong Gu
Lu Li
Jiang Wang
Xiguang Yang
Zhendong Chen

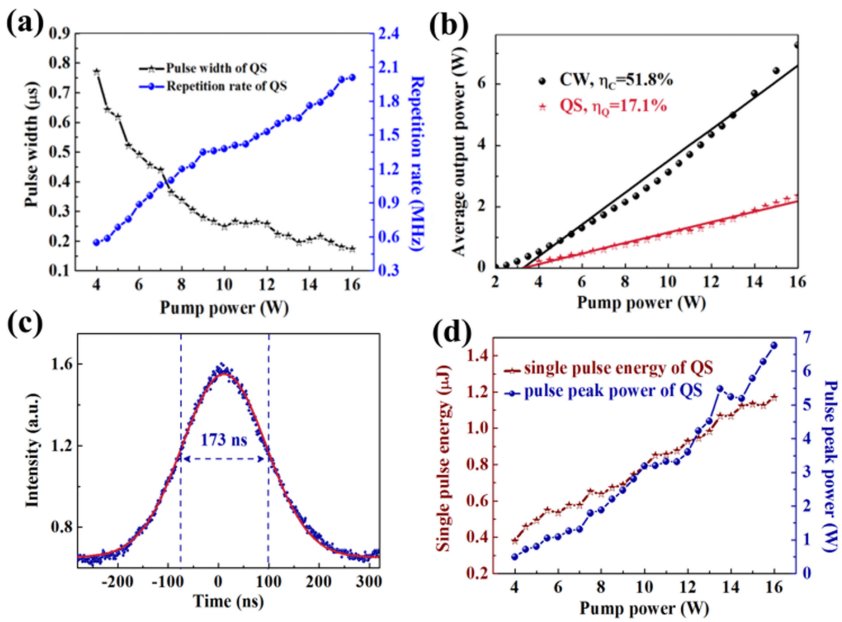

DOI: 10.1109/JPHOT.2019.2900272
1943-0655 © 2019 IEEE

IEEE photonics SOCIETY

IEEE

Titanium Dioxide Langmuir–Blodgett Film Saturable Absorber for Passively Q-switched Nd:$GdVO_4$ Laser

Xi Wang [1,2] Yonggang Wang,[3] Yuzong Gu,[2] Lu Li,[4] Jiang Wang [3] Xiguang Yang,[3] and Zhendong Chen[3]

[1]National Demonstration Center for Experimental Physics and Electronics Education, School of Physics and Electronics, Henan University, Kaifeng 475004, China
[2]School of Physics and Electronics, Henan University, Kaifeng 475004, China
[3]School of Physics and Information Technology, Shaanxi Normal University, Xi'an 710119, China
[4]School of Science, Xi'an University of Posts and Telecommunications, Xi'an 710121, China

DOI:10.1109/JPHOT.2019.2900272

Manuscript received January 21, 2019; revised February 14, 2019; accepted February 15, 2019. Date of publication February 27, 2019; date of current version March 11, 2019. This work was supported by the National Natural Science Foundation of China under Grants 61875053 and 61705183. Corresponding author: Xi Wang (e-mail: chinahnwzwangxi@163.com).

Abstract: A high-transmittance ultra-thin titanium dioxide (TiO_2) film saturable absorber (SA) fabricated by Langmuir–Blodgett (LB) technology is reported and used for the first time to obtain passively Q-switched pulses from a solid-state laser. The optical loss of pure TiO_2 LB film at a wavelength of 1 μm is only 6.5%, and the nonlinear modulation depth, saturation intensity, and non-saturable loss of the entire TiO_2 SA device are 4.3%, 0.125 MW/cm^2, and 9.8%, respectively. Intrinsic high stability and heat resistance of TiO_2 nanomaterials contribute to a laser output with average power (2.35 W) and a corresponding laser pulse width and repetition rate of 173 ns and 2.008 MHz, respectively. The laser output with the pulse energy of 1.17 μJ and peak power of 6.76 W indicates the excellent potential of TiO_2 nanomaterials for applications in solid-state pulsed lasers.

Index Terms: Q-switched laser, saturable absorber, solid-state laser, nonlinear optical materials.

1. Introduction

Thanks to the combination of high average and peak powers, the availability of multifarious laser wavelengths and parameters, and high mechanical stability, pulsed solid-state lasers have captured a significant share of the laser market and are used extensively in some commercial fields, for example, in computer, communication, and consumer electronic (3C) product processing, as well as in experimental and clinical biomedicine, precision metal and non-metal processing, and so on. Among pulsed laser technologies, the generation of passive Q-switching pulse is due to periodical energy mutation caused by the nonlinear saturable absorption of intracavity saturable absorber (SA) device; SAs effectively reduce costs and improve integration compared with active modulation systems [1], [2]. The development of SAs has impelled the diversification of laser pulses. In recent years, following the trend for the development of more flexible and efficient commercial pulsed lasers, new, inexpensive, and high-performance saturable absorption materials have been

investigated, including Graphene [3]–[7], transition-metal dichalcogenides (TMDs) [8]–[13], black phosphorus (BP) [13]–[20], and ferroferric-oxide (Fe_3O_4) [44], [45]. These nano-structured materials possess shorter relaxation times (at the level of picoseconds) than traditional Cr^{4+}:YAG SA (about 3 μs) [37]–[39]; they have better transparency on the premise of guaranteeing excellent nonlinear optical responses, so that they have advantages over traditional semiconductor materials for many applications and almost replace expensive semiconductor saturable absorber mirrors (SESAMs) [2], [21]. In addition, unlike Cr^{4+}:YAG SA (modulation wavelength band of 0.9–1.2 μm) and SESAM [43] (modulated at the specified wavelength), these new nanomaterials SAs can modulate lasers that span a broad range of wavelengths, band from the ultraviolet to the mid-infrared [18], providing new possibilities for the generation of laser pulses in certain wavelength bands. Thus, research on new saturable absorption nanomaterials becomes a hotspot in the field of pulsed lasers.

At present, the intrinsic instability and low thermal-damage threshold of some new nanomaterials is a hindrance to their application in high-power solid-state laser cavities. Compared to previous BP and Fe_3O_4 nanomaterials, titanium dioxide (TiO_2) nanomaterials, as used in our experiment, possess superior thermal stability and can withstand high-intensity laser-induced heat accumulation, solving the problem of thermal damage. As a type of semiconductor material with high dispersibility and transparency, previously, TiO_2 nanomaterials have been used principally as highly efficient photocatalysts, solid-state dye-sensitized solar cells, and biosensors [22], among other applications. In fact, many investigations on the third-order nonlinear optical properties of TiO_2 films such as third-harmonic generation [40], [41] and four-wave mixing [42] have been conducted. Since 2016, in consideration of its several-picosecond recovery time [24], nonlinear optical characteristics [23], [25], and wide absorption band extending to the near-infrared region [26], attempts have been made to utilize TiO_2 in 1-, 1.5-, and 2-μm all-fiber pulsed lasers as SAs [27]–[31]. In these lasers, TiO_2 nanomaterials are embedded within a polymer film like polyvinyl alcohol (PVA) film and sandwiched in between two end-face ferrules of FC fiber connectors. However, the low flatness and heat resistance of TiO_2-polymer film SAs mean that the low insertion-loss and high damage-threshold requirements for solid-state-laser intracavity devices are not met.

In this work, we fabricate a pure TiO_2 Langmuir–Blodgett (LB) film on the surface of a quartz plate, with the aim of avoiding the thermal damage phenomenon from the addition of other materials. Further, LB technology [33], [34] can allow the realization of large-area uniform distributions of a TiO_2 nanomaterial on a substrate, via the exertion of liquid-surface pressure, contributing to the formation of a highly transparent TiO_2 film with a linear optical absorption of 6.5%. The insertion loss of the SA device was also optimized, to values as low as 14%, and the corresponding nonlinear modulation depth, saturation intensity, and non-saturable loss were measured as 4.3%, 0.125 MW/cm^2, and 9.8%, respectively. Based on the outstanding nonlinear optical properties of the prepared TiO_2 SA, Q-switched pulses with widths of 769–173 ns were obtained, corresponding to repetition rates in the range of 0.549–2.008 MHz. The maximum average output power of the Q-switched laser is as high as 2.35 W. To the best of our knowledge, this result represents the best among the previously published reported results for pulsed lasers with TiO_2-based SAs. We calculated that the highest obtainable pulse energy and peak power are 1.17 μJ and 6.76 W, respectively. The realization of a Q-switched pulsed laser verifies the high thermal damage resistance of nonlinear TiO_2 nanomaterial SAs and their potential for application in solid-state pulsed lasers.

2. Preparation and Characterization of TiO_2 SA

A LB membrane system (JML04C1, Powereach, China), including a Langmuir trough, double barriers, and a force transducer, was employed to fabricate the ultra-thin TiO_2 film in this experiment. Details of the fabrication process are illustrated in Fig. 1. TiO_2 powder is dissolved in deionized water with the assistance of a solvent (sodium dodecyl sulfate, SDS) using a liquid phase exfoliation (LPE) method [32]. After ultrasonication and centrifugation, a TiO_2 nanomaterial suspension solution is obtained. In order to improve the dispersal of the TiO_2 nanomaterial over the surface of the subphase in the subsequent film-formation step, we added methanol and chloroform as dispersants to the TiO_2 suspension; for these additions, the volume ratio of suspension:methanol:choloroform

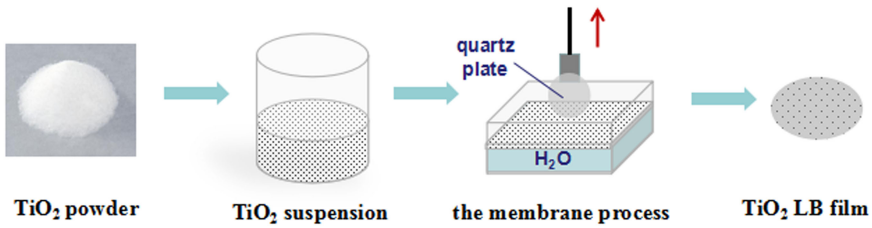

Fig. 1. Fabrication process for TiO_2 LB film.

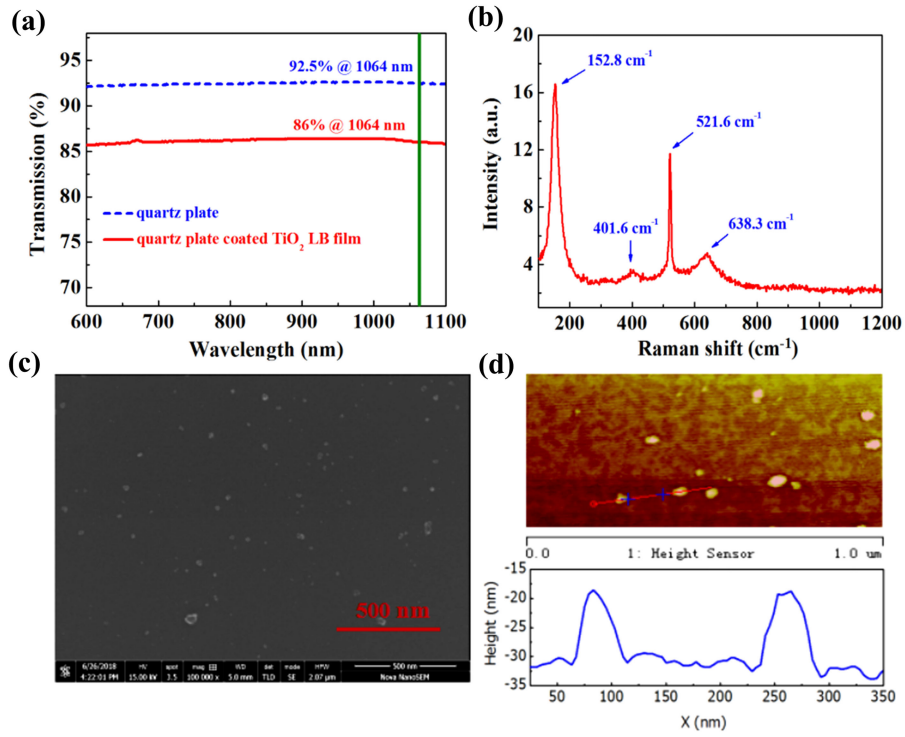

Fig. 2. Characterization of TiO_2 SA device: (a) linear optical transmission, (b) Raman spectrum, (c) SEM image, and (d) AFM image.

was 4:16:3. The deionized water subphase just filled the Langmuir trough, then a 1-mm-thickness hydrophilic quartz plate was fixed on the platinum hanger of a surface pressure detector and slowly vertically dipped into the water subphase in the Langmuir trough. Next, the prepared TiO_2 solution was inserted into the trough at a rate of 0.1 mL/min, so that it dispersed rapidly on the surface of the water subphase. The surface pressure of the air–water interface could be varied by using a pair of mobile barriers to compress the floating TiO_2 Langmuir film. It was demonstrated in this experiment that a surface pressure of 30 mN/m is conducive to the formation of a complete, uniform TiO_2 LB film. Thus, under such surface pressure, the two surfaces of the quartz plate are coated evenly by the TiO_2 nanoplates when it is vertically lifted from the Langmuir trough at a rate of 0.8 mm/min. In order to further reduce the absorption loss of the device, we cleaned off one of the two surface coatings. Finally, the TiO_2 LB SA device was obtained after drying at 80 °C for 24 h.

The linear optical transmission curve of the TiO_2 SA device in the wavelength range of 600–1100 nm was measured using a spectrophotometer. As shown in Fig. 2(a), the transmission spectrum of the pure quartz plate was recorded as a reference, and this displays a flat profile at 92.3 ± 0.3% in the wavelength range of interest; moreover, the transmission of the quartz plate coated

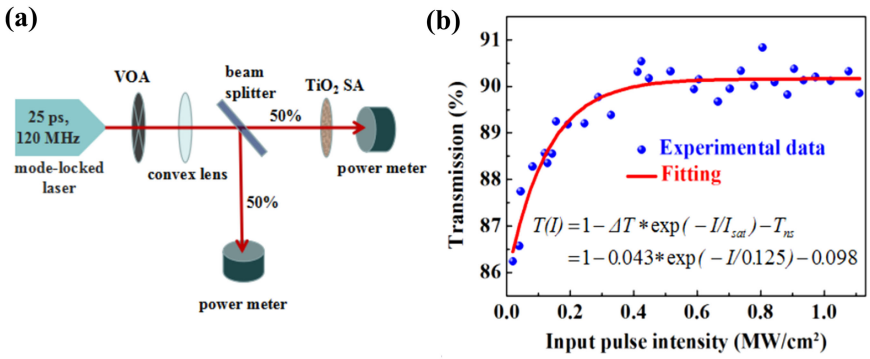

Fig. 3. (a) Schematic diagram of nonlinear optical absorption measurement experiment setup. (b) Nonlinear optical transmission of TiO_2 SA.

with the TiO_2 LB film is also spectrally flat, at 86.1 $\pm$ 0.3%. Taking into consideration the loss of quartz substrate, we compute the linear optical loss of the pure TiO_2 LB film to be 6.5%. We further characterized the TiO_2 LB film, by measuring its Raman spectrum, using a Raman spectrometer excited by a 532-nm laser source; the measured Raman characteristic peaks are shown in Fig. 2(b). Four characteristic peaks located at 152.8, 401.6, 521.6, and 638.3 cm^{-1} represent $E_g(1)$, B_{1g}, A_{1g}, and $E_g(2)$ vibrational modes, respectively, which are indicative of the anatase crystalline structure for TiO_2 [27]. Moreover, in the wavenumber range of 100–3000 cm^{-1} no other Raman peak is present, confirming that no impurities exist in the LB film. We also carried out scanning electron microscopy (SEM) and atomic force microscopy (AFM) of the prepared LB film to characterize the morphology and distribution of the TiO_2 nanomaterial. From the SEM image shown in Fig. 2(c), TiO_2 nanoparticles appear to be flat on the surface of the quartz substrate, evenly distributed on the scale of 500 nm, and the size of the nanoparticles is relatively uniform. The AFM image presented in Fig. 2(d) reveals the thickness and diameter of the TiO_2 nanoparticles as 14 nm and 47 nm, on average, respectively. From the Fig. 2(c) and (d), it can be seen that the distribution of TiO_2 nanoparticles in the film is scattered and the quartz substrate are not fully covered, so the thickness of film equals the thickness of the TiO_2 nanoparticle.

The TiO_2-nanomaterial SAs previously reported exhibit excellent nonlinear optical absorption properties with modulation depths of 30–40% at a laser wavelength of 1.5 μm [27]–[31]. However, high optical absorption caused by such large modulation depths results in too much intracavity loss in a solid-state laser cavity, hindering laser generation. In order to obtain a SA device with low insertion loss for solid state lasers, we prepared the TiO_2 LB film with an optical loss of only 6.5% by the above-mentioned fabrication process. The nonlinear optical transmission properties of the SA device were measured and are displayed in Fig. 3. As shown in Fig. 3(a), the laser source we used to test the new SA is a home-made mode-locked Nd:YVO_4 laser with pulse duration of 25 ps, repetition rate of 120 MHz, and central wavelength of 1064 nm. By using a beam splitter, we extracted a laser beam with half of the total power for use as the SA input reference laser intensity. A variable optical attenuator (VOA) and convex lens are respectively used to continuously alter the input laser power and adjust the spot size on the surface of the SA, and two identical power meters are used to monitor the real-time difference in input and output laser powers synchronously. A series of transmittance data under different input laser intensities was measured and is displayed in Fig. 3(b); the data are fitted with the following function:

$$T(I) = 1 - \Delta T * \exp(-I/I_{sat}) - T_{ns}, \tag{1}$$

where $T(I)$ is the transmission, ΔT is the modulation depth, I is the input laser intensity, I_{sat} is the saturation intensity, and T_{ns} is the non-saturable loss. From the figure we can see that ΔT, I_{sat}, and T_{ns} were calculated as 4.3%, 0.125 MW/cm^2, and 9.8%, respectively. The prepared TiO_2 SA with low non-saturable loss (9.8%) and modulation depth (4.3%) is more suitable for application to

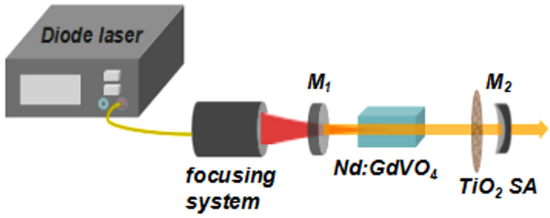

Fig. 4. Schematic diagram of passively Q-switched laser structure.

the solid-state lasers than the previously reported TiO_2-nanomaterial SAs. In addition, compared to chemical vapor deposition (CVD) [35] and pulsed laser deposition (PLD) [36] methods, the low-cost LB processing can be carried out at ambient temperature and atmospheric pressure, which is more suitable for the commercialization of SA device fabrication. Furthermore, the higher the membrane density and thickness are, the larger the value of modulation depth, saturation intensity, and non-saturable loss are. The uniform distribution of TiO_2 nanomaterials in the film is caused by forcing the surface pressure and membrane densities is selected by altering the pressure; the number of film-forming steps determines the film thickness. Thus, there is ample scope for diversity in the development of nonlinear parameters of these films, and the desired nonlinear values can be obtained by controlling the surface pressure and the accumulation of film-forming number.

3. Experimental Setup

The laser cavity structure used in our experiment is illustrated in Fig. 4; the linear cavity has a length of 30 mm. The gain medium is an a-cut Nd:$GdVO_4$ crystal with a Nd^{3+} concentration of 0.3 at.% that is cut into a 3 mm $\times$ 3 mm $\times$ 10 mm cuboid, with the long axis aligned with the laser propagation direction. Both of its light-passing faces are coated with 808-nm and 1064-nm anti-reflection (AR) films to allow sufficient traversal of the pump and oscillating laser. The pump source is an 808-nm fiber-coupled laser diode (LD) with a maximum output power of 30 W, beam waist of 200 μm, and numerical aperture of 0.22. Using an optical focusing system, the size of the pump laser beam when focused onto the Nd:$GdVO_4$ crystal is 400 μm. The end mirror M_1 is a plane dichroic mirror and its surface is coated with an 808-nm high-transmission (HT) film and a 1064-nm high-reflection (HR) film. The end mirror M_2 is not only an output coupler (OC) with a transmission of 9% but also a plano-concave mirror with a radius of curvature of 100 mm that can alter the spot size on the SA. The TiO_2 SA was inserted between M_2 and the gain crystal. By simulations based on ABCD propagation matrix theory, the laser beam radius in the gain medium was obtained as in the range of 116–117.5 μm, and the spot radius on the surface of SA varies between 118 and 129 μm with the fine tuning of the position of the SA. During normal laser operation, the Nd:$GdVO_4$ crystal is maintained at 20 °C by a cool-water machine to minimize thermal lensing effects.

4. Experimental Results and Discussion

By fine tuning the alignment of the cavity mirrors and enhancing the pump power, continuous wave (CW) operation with a lasing threshold of 2 W was obtained. Next, we inserted the prepared TiO_2 SA into the laser cavity and optimized the laser output by further increasing the power of the pump, also changing the distance between the SA and M_2, until Q-switched (QS) pulses appeared. Figure 5 displays the stable QS pulse trains under pump powers of 4, 7, 10, 13, and 16 W. The pulsed generation is due to the sudden depress of laser oscillation threshold caused by fully saturated absorption of SA. After the first pulse outputs, the absorption of SA return to high initial value, and the inverted population can be re-accumulated in preparation for the formation of next pulse. According to the passive Q-switching principle, under higher pump power, shorter saturation absorption period of SA and stronger stimulated radiation would contribute to the generation of

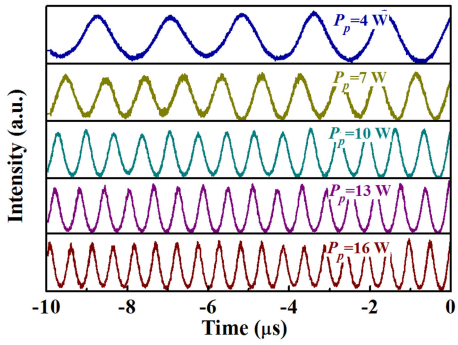

Fig. 5. Pulse trains of Q-switched laser under different pump powers.

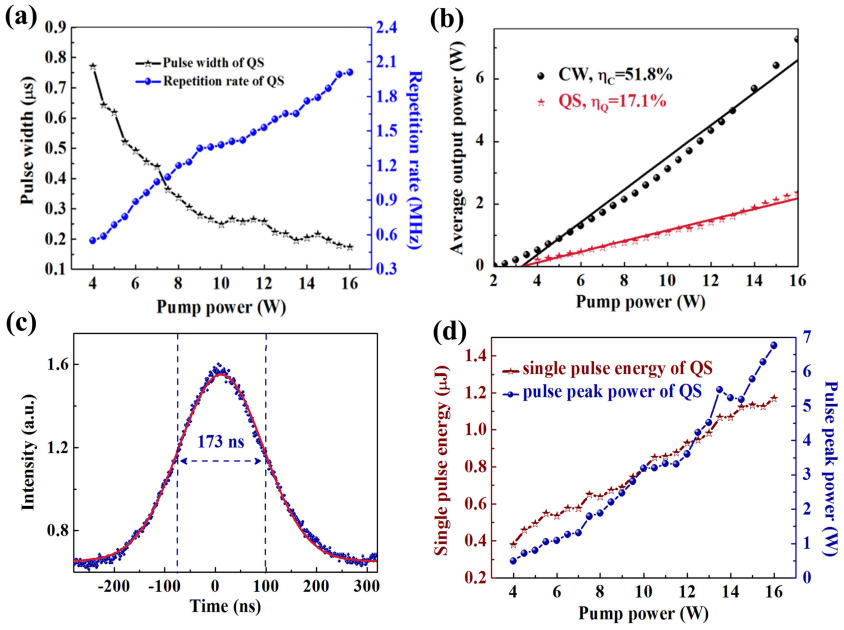

Fig. 6. (a) Evolution of repetition rate and pulse duration with pump power. (b) Average output powers of CW and QS versus pump power. (c) The narrowest single pulse. (d) Single pulse energy and peak power versus pump power.

pulses with higher repetition rate and narrower pulse width, respectively. Therefore, it can be seen from Fig. 5 that QS pulse durations become narrower with increasing pump power, while the number of pulses occurring in the same period of time increases. Figure 6(a) shows the evolution of pulse width and repetition rate versus pump power. The repetition rate curve presents a continuous upward trend, from 0.549 to 2.008 MHz, as pump power increases from 4 to 16 W, the width of a single pulse drops from 769 to 173 ns. Then, we calculated the amplitude jitter rate to characterize the amplitude stability of QS pulses. Based on the function,

$$R_a = \left| \frac{A_i - \overline{A}}{\overline{A}} \right|_{\max} \times 100\%, \tag{2}$$

where R_a is the amplitude jitter rate, $\bar{A}$ is the average amplitude, A_i is the amplitude of pulse. The measured amplitude jitter rate is 1.9%.

TABLE 1
Passively Q-switched Lasers with the TiO_2 SAs

SA type	Gain medium	Wavelength (nm)	Pulse width	Repetition rate (kHz)	Average output power	Pulsed energy	Peak power	Ref
TiO_2-polymer film	erbium-doped fiber	1558	1.8 μs	20.5	~0.25 mW	~2.2 nJ	~1.1 mW	29
TiO_2-polymer film	ytterbium-doped fiber	1036	4.3 μs	86.7	0.15 mW	1.7 nJ	–	30
TiO_2-polymer film	ytterbium-doped fiber	1039	3.2 μs	64.5	0.13 mW	2 nJ	–	31
TiO_2 LB film	Nd:$GdVO_4$	1064	173 ns	2008	2.35 W	1.17 μJ	6.76 W	

During the experiments, the average output powers of the CW and QS lasers were measured as a function of pump power, with measurements recorded over a pump power range of 2–16 W at intervals of 0.5 W (Fig. 6(b)). It is apparent from the figure that both groups of average output power increase approximately linearly with pump power, by ignoring a few abnormal data caused by thermal lensing effect of the gain medium and the slight jitter of pump power. After linear fitting, the slope efficiencies of the CW and QS lasers are 51.8% and 17.1%, respectively. The slope efficiency of QS laser is less than that of CW laser, which mainly attributes to the loss from non-saturable absorption of TiO_2 SA. Thus, in order to increase the slop efficiency and output power of Q-switched laser, future design of new emerging SAs should focus on the decrease of non-saturable absorption loss, including the selection of higher transmittance substrate and the optimization of nanomaterials' thickness. For a pump power of 16 W, the maximum average output power of the QS laser approaches 2.35 W. Due to a thermal lensing effect of the gain medium caused by high-intensity pump-laser irradiation, the intracavity laser beam size changes and laser operation transforms from QS into CW when the pump power exceeds 16 W. Thus, the narrowest pulse, with a duration of 173 ns, is achieved at a pump power of 16 W and its profile is displayed in Fig. 6(c).

Based on the average-output-power, pulse-width, and repetition-rate data, we calculated the corresponding single pulse energies and peak powers of the QS laser. The variation of these calculated values with pump power are presented in Fig. 6(d). Ignoring a few abnormal data outliers, both single pulse energy and peak power increase with the power of the pump, confirming that our laser output is of the QS mode rather than the relaxation oscillation mode; in the latter mode, although the repetition rate increases with pump power, the peak power does not. The largest single pulse energy, 1.17 μJ, and the highest peak power, 6.76 W, were obtained when the pump power was 16 W.

In this study, we applied an as-fabricated TiO_2 SA to a solid state laser cavity for the first time. Unlike previously reported TiO_2-polymer composite film SAs used in fiber lasers, our TiO_2 SA device was fabricated by uniformly distributing the TiO_2 nanomaterials on the surface of a quartz plate using the LB film-forming method. Without the addition of polymer materials that have low flatness and heat resistance, the pure-TiO_2 LB-film SA exhibits excellent an modulation depth of 4.3% and a lower non-saturable loss of 9.8%; in addition, TiO_2 nanomaterials possess intrinsic stability and high thermal damage thresholds, avoiding the thermal damage problems of SA devices used in high-intensity lasers, and contributing to the generation of passive Q-switching pulses in solid-state lasers. The detailed comparison between passive Q-switching operations by the TiO_2-polymer film SA and our laser result are exhibited in Table 1. Compared to previously reported work, our Q-switched pulses have higher average output power, peak power, and pulse energy, verifying the superiority of the TiO_2 LB-film SA and its application potential in pulsed solid-state lasers. Additionally, both the pulse width of 173 ns and repetition rate of 2.008 MHz are also the best results among Q-switched lasers based on TiO_2 SA so far.

Table 2 shows several representative Q-switching laser results at 1 μm spectral region based on various new nanomaterials SAs. From the Table, we can see that the average output power and pulsed energy values obtained in our work are higher than the lasers results operated by BP

TABLE 2
Passively Q-switched Solid State Lasers at 1 μm Wavelength Based on Different SAs

SA	Gain medium	Wavelengh (nm)	Repetition rate (kHz)	Pulse width (ns)	Output power (mW)	Pulsed energy (μJ)	Ref
Graphene SA mirror	Nd:$GdVO_4$	1063	704	105	2300	3.3	46
Graphene glass substrate	Nd:LYSO	1079	159	96	1800	11.3	6
WS_2 SA	Nd:YVO_4	1064	1030	56	1360	1.3	10
MoS_2 substrate	Yb:LGGG	1025-1028	333	182	600	1.8	47
BP-based SA mirror	Yb:$CaYAlO_4$	1046	113.6	620	37	0.33	20
Fe_3O_4 solution SA	Nd:YVO_4	1064.4	576.4	53	104	0.18	45

and Fe_3O_4 SAs. It is mainly due to that TiO_2 nanomaterial possess more superior thermal stability and higher damage resistance than BP and Fe_3O_4 nanomaterials. However, our laser parameters including the pulse width and pulsed energy still lag behind the QS lasers with Graphene and TMDs SAs. So far, the two latter SAs have been relatively maturely used in the generation of passive Q-switched pulsed lasers; the reported Q-switching pulsed energy and corresponding pulse width have been already above 10 μJ and below 100 ns, respectively [6]. As a kind of new SA, TiO_2 nanomaterial exhibits ultrashort recovery time (1.5 ps), excellent saturable absorption, and high thermal stability, therefore, its application potential in pulsed laser is competitive with the Graphene and TMDs. In order to make full use of the excellent nonlinear performance of TiO_2 nanomaterials, and further enhance the laser output energy and power, our next research focus is to optimize the modulation depth and non-saturable loss as well as improve the controllability and stability of nonlinear parameters.

5. Conclusion

In summary, a highly stable and heat-resistant TiO_2-nanomaterial SA was used for pulse modulation in a passively Q-switched solid state laser for the first time. Utilizing LB film-forming technology, we fabricated a TiO_2 SA device with a nonlinear modulation depth of 4.3%, saturation intensity of 0.125 MW/cm^2, and non-saturable loss of 9.8%, conforming with the high-transmission requirement of laser devices for solid state lasers. By inserting the SA into a laser cavity, the pulse width of the obtained Q-switched laser is in the range between 769 and 173 ns, and the corresponding repetition rates vary from 0.549 to 2.008 MHz. It is noted that the maximum laser average output power reaches 2.35 W, and the corresponding pulse energy and peak power are as high as 1.17 μJ and 6.76 W, respectively, which indicates good application potential for TiO_2 nanomaterials for the generation of large energy pulses in solid state lasers as well as the superiority of traditional LB technology for high-quality ultra-thin film formation.

References

[1] U. Keller, D. Miller, G. Boyd, T. Chiu, J. Ferguson, and M. Asom, "Solid-state low-loss intracavity saturable absorber for Nd:YLF lasers: an antiresonant semiconductor Fabry-Perot saturable absorber," *Opt. Lett.*, vol. 17, no. 7, pp. 505–507, 1992.
[2] U. Keller *et al.*, "Semiconductor saturable absorber mirrors (SESAM's) for femtosecond to nanosecond pulse generation in solid-state lasers," *IEEE J. Sel. Topics Quantum Electron.*, vol. 2, no. 3, pp. 435–453, Sep. 1996.
[3] A. Geim, "Graphene: Status and prospects," *Science*, vol. 324, pp. 1530–1534, 2009.
[4] P. Avouris, "Graphene: Electronic and photonic properties and devices," *Nano Lett.*, vol. 10, no. 11, pp. 4285–4294, 2010.
[5] Q. Bao *et al.*, "Atomic-layer graphene as a saturable absorber for ultrafast pulsed lasers," *Adv. Functional Mater.*, vol. 19, pp. 3077–3083, 2009.

[6] Y. Zhao *et al.*, "Dual-wavelength synchronously Q-switched solid-state laser with multi-layered graphene as saturable absorber," *Opt. Exp.*, vol. 21, no. 3, pp. 3516–3522, 2013.
[7] Q. Wang *et al.*, "Graphene on SiC as a Q-switcher for a 2 μm laser," *Opt. Lett.*, vol. 37, no. 3, pp. 395–397, 2012.
[8] Q. Wang, K. Kalantar-Zadeh, A. Kis, J. Coleman, and M. Strano, "Electronics and optoelectronics of two-dimensional transition metal dichalcogenides," *Nature Nanotechnol.*, vol. 7, no. 11, pp. 699–712, 2012.
[9] K. Wang *et al.*, "Ultrafast saturable absorption of two-dimensional MoS_2 nanosheets," *ACS Nano*, vol. 7, no. 10, pp. 9260–9267, 2013.
[10] W. Tang *et al.*, "1.36 W passively Q-switched YVO_4/Nd: YVO_4 laser with a WS_2 saturable absorber," *IEEE Photon. Technol. Lett.*, vol. 29, no. 5, pp. 470–473, Mar. 2017.
[11] L. Li *et al.*, "WS_2/fluorine mica (FM) saturable absorbers for all-normal-dispersion mode-locked fiber laser," *Opt. Exp.*, vol. 23, no. 22, pp. 28698–28706, 2015.
[12] B. Xu *et al.*, "Passively Q-switched Nd:$YAlO_3$ nanosecond laser using MoS_2 as saturable absorber," *Opt. Exp.*, vol. 22, no. 23, pp. 28934–28940, 2014.
[13] P. Ge, J. Liu, S. Jiang, Y. Xu, and B. Man, "Compact Q-switched 2 μm Tm:$GdVO_4$ laser with MoS_2 absorber," *Photon. Res.*, vol. 3, no. 5, pp. 256–259, 2015.
[14] S. Lu *et al.*, "Broadband nonlinear optical response in multilayer black phosphorus: an emerging infrared and mid-infrared optical material," *Opt. Exp.*, vol. 23, no. 9, pp. 11183–11194, 2015.
[15] J. Sotor, G. Sobon, M. Kowalczyk, W. Macherzynski, P. Paletko, and K. Abramski, "Ultrafast thlium-doped fiber laser mode locked with black phosphorus," *Opt. Lett.*, vol. 40, no. 16, pp. 3885–3888, 2015.
[16] Z. Qin *et al.*, "Black phosphorus as saturable absorber for the Q-switched Er:ZBLAN fiber laser at 2.8 μm," *Opt. Exp.*, vol. 23, no. 19, pp. 24713–24718, 2015.
[17] X. Wang, Z. Wang, Y. Wang, L. Li, G. Yang, and J. Li, "Watt-level high-power passively Q-switched laser based on a black phosphorus solution saturable absorber," *Chin. Opt. Lett.*, vol. 15, no. 1, p. 011402, 2017.
[18] L. Kong *et al.*, "Black phosphorus as broadband saturable absorber for pulsed lasers from 1 μm to 2.7 μm wavelength," *Laser Phys. Lett.*, vol. 13, no. 4, 2016, Art. no. 045801.
[19] B. Zhang *et al.*, "Exfoliated layers of black phosphorus as saturable absorber for ultrafast solid-state laser," *Opt. Lett.*, vol. 40, no. 16, pp. 3691–3694, 2015.
[20] J. Ma *et al.*, "Few-layer black phosphorus based saturable absorber mirror for pulsed solid-state lasers," *Opt. Exp.*, vol. 23, no. 17, pp. 22643–22648, 2015.
[21] A. Diebold *et al.*, "SESAM mode-locked Yb:$CaGdAlO_4$ thin disk laser with 62 fs pulse generation," *Opt. Lett.*, vol. 38, no. 19, pp. 3842–3845, 2013.
[22] J. Liu *et al.*, "Stacked graphene-TiO_2 photoanode via electrospray deposition for highly efficient dye-sensitized solar cells," *Organic Electron.*, vol. 23, pp. 158–163, 2015.
[23] Y. Jiang *et al.*, "Abnormal nonlinear optical properties of hybrid graphene-TiO_2 nanostructures," *Opt. Lett.*, vol. 43, no. 3, pp. 523–526, 2018.
[24] H. Elim, W. Ji, A. Yuwono, J. Xue, and J. Wang, "Ultrafast optical nonlinearity in PMMA-TiO_2 nanocomposites," *Appl. Phys. Lett.*, vol. 82, pp. 2691–2693, 2003.
[25] K. Iliopoulos, G. Kalogerakis, D. Vernardou, N. Katsarakis, E. Koudoumas, and S. Couris, "Nonlinear optical response of titanium oxide nanostructured thin films," *Thin Solid Films*, vol. 518, no. 4, pp. 1174–1176, 2009.
[26] K. Reddy, S. Manorama, and A. Reddy, "Bandgap studies on anatase titanium dioxide nanoparticles," *Mater. Chem. Phys.*, vol. 78, no. 1, pp. 239–245, 2003.
[27] M. Rusdia *et al.*, "Titanium dioxide (TiO_2) film as a new saturable absorber for generating mode-locked Thulium-Holmium doped all-fiber laser," *Opt. Laser Technol.*, vol. 89, pp. 16–20. 2017.
[28] Z. Salleh *et al.*, "Mode-locked erbium-doped fiber laser with titanium dioxide saturable absorber," *Dig. J. Nanomater. Biostruct.*, vol. 11, no. 4, pp. 1173–1178, 2016.
[29] H. Ahmad *et al.*, "C-Band Q-Switched fiber laser using titanium dioxide (TiO_2) as saturable absorber," *IEEE Photon. J.*, vol. 8, no. 1, Feb. 2016, Art. no. 1500107.
[30] H. Ahmad and M. A. M. Salim, "TiO_2-Based Q-switched ytterbium-doped fiber laser," *IEEE J. Quantum Electron.*, vol. 53, no. 5, Oct. 2017, Art. no. 1600306.
[31] H. Ahmad *et al.*, "Titanium dioxide-based Q-switched dual wavelength in the 1 micron region," *Chin. Opt. Lett.*, vol. 14, no. 9, 2016, Art. no. 091403.
[32] J. Coleman *et al.*, "Two-dimensional nanosheets produced by liquid exfoliation of layered materials," *Science*, vol. 331, pp. 568–571, 2011.
[33] J. Zasadzinski, R. Viswanathan, L. Madsen, J. Garnaes, and D. Schwartz, "Langmuir-Blodgett films," *Science*, vol. 263, pp. 1726–1733, 1994.
[34] X. Li *et al.*, "Highly conducting graphene sheets and Langmuir-Blodgett films," *Nature Nanotechnol.*, vol. 3, no. 9, pp. 538–542, 2008.
[35] W. Ren, L. Gao, L. Ma, and H. Cheng, "Preparation of graphene by chemical vapor deposition," *New Carbon Mater.*, vol. 26, no. 1, pp. 71–80, 2011.
[36] Y. Suda, H. Kawasaki, T. Ueda, and T. Ohshima, "Preparation of high quality nitrogen doped TiO_2 thin film as a photocatalyst using a pulsed laser deposition method," *Thin Solid Films*, vol. 453, pp. 162–166, 2004.
[37] J. Zheng, S. Zhao, and L. Chen, "Laser-diode end-pumped passively Q-switched Nd: YVO_4 laser with Cr^{4+}:YAG saturable absorber," *Opt. Eng.*, vol. 41, no. 9, pp. 2271–2276, 2002.
[38] J. Dong, K. I. Ueda, A. Shirakawa, H. Yagi, T. Yanagitani, and A. A. Kaminskii, "Composite Yb:YAG/Cr^{4+}:YAG ceramics picosecond microchip lasers," *Opt. Exp.*, vol. 15, no. 22, pp. 14516–14523, 2007.
[39] B. Cole, L. Goldberg, C. W. Trussell, A. Hays, B. W. Schilling, and C. McIntosh, "Reduction of timing jitter in a Q-Switched Nd:YAG laser by direct bleaching of a Cr^{4+}:YAG saturable absorber," *Opt. Exp.*, vol. 17, no. 3, pp. 1766–1771 2009.
[40] T. Hashimoto, T. Yoko, and S. Sakka, "Sol–gel preparation and third-order nonlinear optical properties of TiO_2 thin films," *Bull. Chem. Soc. Jpn.*, vol. 67, no. 3, pp. 653–660, 1994.

[41] S. K. Das *et al.*, "Highly efficient THG in TiO_2 nanolayers for third-order pulse characterization," *Opt. Exp.*, vol. 19, no. 18, pp. 16985–16995, 2011.
[42] Q. Zhou, Q. Zhang, J. Zhang, L. Zhang, and X. Yao, "Preparation and optical properties of TiO_2 nanocrystalline particles dispersed in SiO_2 nano-composites," *Mater. Lett.*, vol. 31, pp. 39–42, 1997.
[43] B. Braun, F. X. Kärtner, G. Zhang, M. Moser, and U. Keller, "56-ps passively Q-switched diode-pumped microchip laser," *Opt. Lett.*, vol. 22, no. 6, pp. 381–383, 1997.
[44] X. Bai *et al.*, "Passively Q-switched erbium-doped fiber laser using Fe_3O_4-nanoparticle saturable absorber," *Appl. Phys. Exp.*, vol. 9, no. 4, 2016, Art. no. 042701.
[45] X. Wang, Y. Wang, D. Mao, L. Li, and Z. Chen, "Passively Q-switched Nd: YVO_4 laser based on Fe_3O_4 nanoparticles saturable absorber," *Opt. Mater. Exp.*, vol. 7, no. 8, pp. 2913–2921, 2017.
[46] X. Li, J. Xu, Y. Wu, J. He, and X. Hao, "Large energy laser pulses with high repetition rate by graphene Q-switched solid-state laser," *Opt. Exp.*, vol. 19, no. 10, pp. 9950–9955, 2011.
[47] F. Lou, *et al.*, "Nanosecond-pulsed, dual-wavelength, passively Q-switched ytterbium-doped bulk laser based on few-layer MoS_2 saturable absorber," *Photon. Res.*, vol. 3, no. 2, pp. A25–A29, 2015.